Journal of Materials, Processing and Design (2024)
Clausius Scientific Press, Canada

DOI: 10.23977/jmpd.2024.080204
ISSN 2516-0923 Vol. 8 Num. 2

Bio-tribological properties of GQDs@Si_3N_4 composite ceramics for hip joint

Yu Tian[1,a], Wei Chen[1,b,*], Kun Cheng[1,c], Zhuohao Sun[1,d], Yucheng Ma[1,e], Zehao Li[1,f], Shuai Wang[1,g]

[1]College of Mechanical and Electrical Engineering, Shaanxi University of Science & Technology, Xi'an, Shaanxi, 710021, China

[a]2794993539@qq.com, [b]chenweijd@sust.edu.cn, [c]1393182072@qq.com, [d]1424878458@qq.com, [e]2506078508@qq.com, [f]1109222159@qq.com, [g]1916215085@qq.com

[*]Corresponding author.

Keywords: N-GQDs, Bioceramic, Wear resistance, Artificial joint material

Abstract: In order to find new artificial hip joint replacement materials with good mechanical properties and wear resistance, one Si_3N_4 (silicon nitride) - based ceramic composite with addition of N-GQDs (which was transformed from nano-lignin precursor in the process) was developed in this study. The biological wear resistance of the ceramic composite sliding against common polymer medical material (HXLPE, UHMWPE and PEEK) in calf serum solution was systematically studied in this paper. Results showed that, when the ceramic composite slid against HXPLE, a black surface film containing silica gel and N-GQDs formed in the sliding process. The formation of this film effectively inhibited the direct contact between the surface of ceramic and polymer, and the wear rate of HXLPE against the composite was 82% lower than that against single-phase Si_3N_4. The poor wear resistance of HXLPE disc against single-phase Si_3N_4 was mainly attributed to its weak strength and toughness and the absence of N-GQDs. When the ceramic composite slid against UHMWPE and PEEK, due to rough wear surface of the latter two was formed during the sliding process, and no effective protective film formed, so the wear rates of the UHMWPE and PEEK discs were higher than that of HXLPE. In general, the composite has great application potential in the field of artificial hip replacement materials.

1. Introduction

In order to reduce the pain of patients with arthritis and joint injury, total hip arthroplasty (THA) has been popularized around the world, and the service reliability and stability of artificial hip joint materials will inevitably affect the diagnosis and treatment effect of joint replacement and the quality of life of patients [1-3]. Ceramic materials have good mechanical properties, wear resistance and biocompatibility, and have become the mainstream joint replacement materials. In particular, silicon nitride ceramics (Si_3N_4) have good phase stability and osteogenic properties [4-11],and have been

used in the medical field of cervical spacers and spinal fusion devices since 2008[10,12]. However, when ceramic materials are used in total hip arthroplasty, because of the heavy load and frequent friction of the hip joint, the surface of the artificial joint is prone to abnormal noise and fragmentation due to friction, which greatly affects the physical and mental health of patients. Therefore, the development of new ceramic-based self-lubricating bio-ceramic materials has been a research hotspot in the field of artificial joint replacement.

A large number of studies have shown that graphene material can effectively improve the friction and wear properties of Si_3N_4 ceramics as a second phase. For example, when Llorente et al. [13] studied the friction and wear properties of Si_3N_4/GNPs composites under isooctane lubrication, it was found that the addition of 20vol.%GNPs reduced the friction coefficient of the composites by 50% compared with single-phase silicon nitride, and the wear resistance increased by 63%. At the same time, Belmonte et al. [14] also found that the addition of 3wt%GNPs to the Si_3N_4 composite increased its wear resistance by 56% under the condition of isooctane lubrication. Hvizdos et al. [15] also found that the addition of 3wt%GNPs improved the wear resistance of Si_3N_4 ceramics, but its friction coefficient was not significantly reduced. In addition, Rutkowski et al. [16] pointed out that when the graphene added phase content was 2-10wt%, the friction and wear properties of the composite were not improved, but the addition of graphene worsened the tribological performance. From the available data, it can be seen that due to the different starting points of scholars and different test schemes, the test results lack consistency and contrast. Obviously, due to the intrinsic physical structure and poor dispersion of graphene, its use as an additive phase to improve the tribological properties of silicon nitride ceramics lacks stability and reliability. Therefore, it is urgent to search for a highly dispersed and controlled graphene precursor as the second phase to improve the friction and wear properties of silicon nitride ceramics.

Lignin, a typical biomass material, can be pyrolytically transformed into graphene material under certain conditions. Li et al. [17] had found that sulfate lignin could be pyrolyzed and oxidized to graphene oxide under the action of ferric nitrate catalyst. Ishii et al. [18] firstly obtained iron-supported lignin by freeze-drying, and then catalyzed carbonization at 1200℃ to obtain graphene materials. At the same time, Liu et al. [19] also pyrolyzed sulfate lignin to multilayer graphene and carbon nanotubes at 1000℃. More interestingly, lignin can also be pyrolyzed into graphene quantum dots (GQDs) under certain conditions. For example, Temerov et al. [20] prepared graphene quantum dots using lignin as carbon source using a top-down method. Liu et al. [21] prepared lignin-derived graphene quantum dots (P-LGQD) by phosphoric acid-assisted hydrothermal method, with particle sizes ranging from 4-6nm and lattice spacing of 0.251nm. Graphene quantum dots (GQDs), as a new type of carbon nanomaterials, have high surface area, excellent biocompatibility, low toxicity and fluorescence properties, and are mainly concerned and applied in the fields of medical sensing, detection and optoelectronics [22,23].

Our research group innovatively introduced nano lignin as a precursor of N-GQDs into silicon nitride ceramic matrix, and prepared ceramic matrix composite material containing N-GQDs through pyrolysis conversion and hot pressing sintering. The results showed that the composite had excellent fracture toughness (9.08±0.23 $MPa \cdot m^{1/2}$) and flexural strength (988.98±18.77MPa). When the composite material slid against nickel-based superalloy, its dry friction coefficient was only 0.22, and the wear rate was only $1.74\times10^{-6} mm^3/N \cdot m$. The mechanical properties and microstructure characterization of the composite ceramics were described in the previously published literature [24]. Compared with single-phase silicon nitride, the composite exhibited better mechanical properties and

wear properties. Therefore, the composite should have great potential as a material for artificial joint replacement.

In view of this, this paper focuses on studying the biological wear properties of silicon-nitride composites containing lignin precursors in calf serum solution, revealing the wear properties of silicon-nitride composites paired with commonly used biopolymers, and clarifying the mechanism of N-GQDs in low wear behavior. This work provides a new design idea for the development of new artificial hip joint materials, and provides new data support for expanding the tribological research of ceramic materials

2. Experimental procedure

2.1 Material preparation

In this study, high purity Si_3N_4 powder (average particle size of 0.5μm, purity > 99%) was used as the main raw material, nano lignin was used as the second phase precursor, and 6wt%Al_2O_3 (average particle size of 1.17μm) and 4wt%Y_2O_3 (average particle size of 0.37μm) were used as sintering additives. Among them, nano lignin was extracted from wheat straw by deep eutectic solvent (DES) method, and its particle size was 50-150nm. The addition amount of nano-lignin was 2wt.%, the sample was labeled SN-2L, and the single-phase silicon nitride was labeled SN0.

The preparation of new composite materials was mainly divided into two steps: mixing and pyrolytic-hot press sintering, as detailed in reference [24,25]. In the mixing process, firstly, all the original powder was weighed proportionally and poured into the ball mill tank; Then, the original powder was ball milled for 3h at a speed of 150r/min in ethanol medium. Subsequently, the mixed powder was dried in an oven at 50℃ for 8h; Finally, the mixed powder was sieved using an 80-mesh stainless steel screen to obtain an evenly mixed original powder. In the process of pyrolytic-hot press sintering, the mixed powder was first loaded into a special graphite mold; After that, the graphite mold containing the mixed powder was placed in the hot pressing sintering furnace (ZTY 40-21Y, Shanghai Chenhua Technology Co., LTD.) for pyrolysis and hot pressing sintering. The specific process was shown in Figure 1, the composite powder was gradually heated to 800℃, 1400℃ and 1700℃, and the discs sample with the size of Φ44mm×6mm were prepared by sintering. Finally, the sintered samples were cut into the pin samples with a size of 5mm×5mm×15mm using a diamond cutting machine.

The commercially purchased ultra-high molecular weight polyethylene (UHMWPE), highly crosslinked polyethylene (HXLPE) and polyether ether ketone (PEEK) materials were used as disc samples, the size of which was Φ44mm×6mm. UHMWPE and HXLPE were purchased from Beijing Chunlizhengda Medical Equipment Co., LTD. PEEK was purchased from Shanghai Chaoju New Materials Co., LTD. Refer to ISO21534-2007 [26], composite ceramic pin samples and polymer disc samples were polished, and the surface roughness of composite material pin samples and disc samples was not higher than Ra0.1μm and Ra0.2μm, respectively.

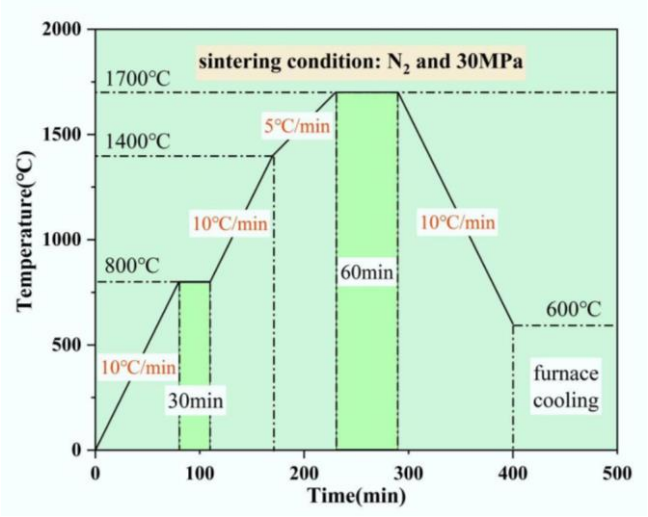

Figure 1: The schematic diagram of sintering process for the composite.

2.2 Construction of biological environment

In order to simulate the media environment of human joint cavity, calf serum solution (provided by Nanjing Vicente Biotechnology Co., LTD.) was used to create the media environment. Before the friction and wear test, amphotericin B (25mg/L), dimethyl sulfoxide (1ml/L) and gentamicin (2ml/L) were added to calf serum solution to inhibit bacterial growth. At the same time, EDTA (concentration 7.5g/L) was also added to the serum to reduce the precipitation of calcium phosphate between the friction interfaces. Finally, the prepared solution was diluted with deionized water to obtain a suitable biological medium solution with a protein concentration of 20g/L [27].

2.3 Biological wear testing

In this study, BiotriboPOD-M732 (Orthotek Laboratory, Shanghai, China) was used to carry out the biological tribological wear test. The principle diagram of the testing machine is shown in Figure 2, the hydraulic driver is used to exert normal load on the pin sample, and the disc sample is rotated to realize the pin-disc wear process. According to ASTM F732 [28], biological wear test parameters were set in this study, and the specific parameter values are shown in Table 1. At the same time, according to ISO14242-1:2014 and ISO14242-2:2016[27,29], the polymer disc samples were soaked in deionized water before the wear test to ensure that they were saturated with water absorption. The number of cycles of the biological wear test was 1 million (1Mc), and the four stages of the phased study were 0.25Mc, 0.5Mc, 0.75Mc and 1Mc. After the biological wear test, the wear surfaces of the pin and disc samples were cleaned by ultrasonic cleaning instrument, the surface roughness before and after wear was measured by ultra-depth of field microscope (DSX510, Olympus, Japan), and the samples before and after wear were weighed by electronic balance (ME55, accuracy 0.01mg) to calculate the wear amount and volume wear rate. The wear rate is calculated as $V_m=\Delta m/FS\rho$, where Δm represents the mass loss after wear, F is the normal load, S is the sliding distance, and ρ is the sample density.

Table 1: Test parameters of wear experiment.

Test parameter	Detail
normal load	2MPa
lubricating condition	calf serum solution
motion form	circular motion
rotational frequency	1Hz
radius of motion	5mm
angular velocity	6.28rad/s
test temperature	37±2℃
cycle index	1000000

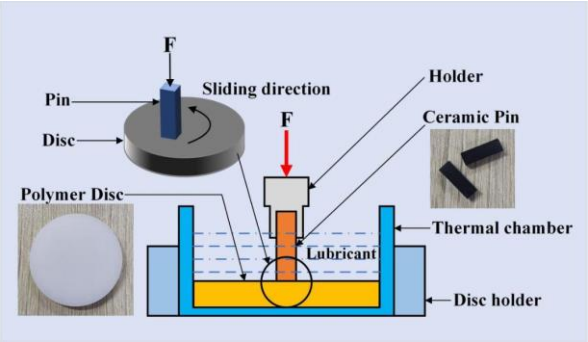

Figure 2: Schematic diagram of implant material wear testing machine.

2.4 Characterization techniques

In this study, scanning electron microscope (SEM, Verios 460, USA) was used to observe the worn surface morphology of the sample, and OCTANE PLUS energy spectrometer (EDS) equipped with Verios 460 was used to analyze the chemical element composition of the sample surface. In addition, the roughness of the worn surface of the sample was measured by ultra-depth of field optical microscopy (DSX510, Olympus, Japan), and the material composition of the worn surface was analyzed by X-ray photoelectron spectroscopy (XPS, K-Alpha, USA) and laser micro-Raman spectroscopy (Raman, DXRxi, USA).

3. Results and discussion

In this study, when ceramic pins slid against UHMWPE, HXLPE and PEEK discs, the ceramic pin sample has almost no wear due to its relatively high hardness and wear resistance. Therefore, in this study, the wear data of polymer disc samples were used to evaluate the biological wear properties of composite ceramics as joint accessories.

Figure 3 shows the mass loss and volume wear rate of the polymer discs under different cycles. As shown in Figure 3 (a), the mass loss of polymer disc increases with the increase of the number of cycles, and the increase of mass losses of discs sliding against SN-2L composite ceramics are significantly lower than that of discs sliding against single-phase silicon nitride (SN0). As shown in Figure 3 (b), the volume wear rate of polymer discs sliding against composite ceramics are significantly lower than those of polymer discs sliding against SN0 ceramics, and the wear rate of HXLPE disc sliding against SN-2L pin significantly decreases with the increase of cycle times. When

the cycle number is 1Mc, the wear rates of HXLPE, UHMWPE and PEEK discs sliding against SN-2L are $0.18\times10^{-6}mm^3/N\cdot m$, $5.21\times10^{-6}mm^3/N\cdot m$ and $0.58\times10^{-6}mm^3/N\cdot m$, respectively. Compared with SN0/polymer pairs, the wear rates of discs are reduced by 82%, 53% and 59%, respectively.

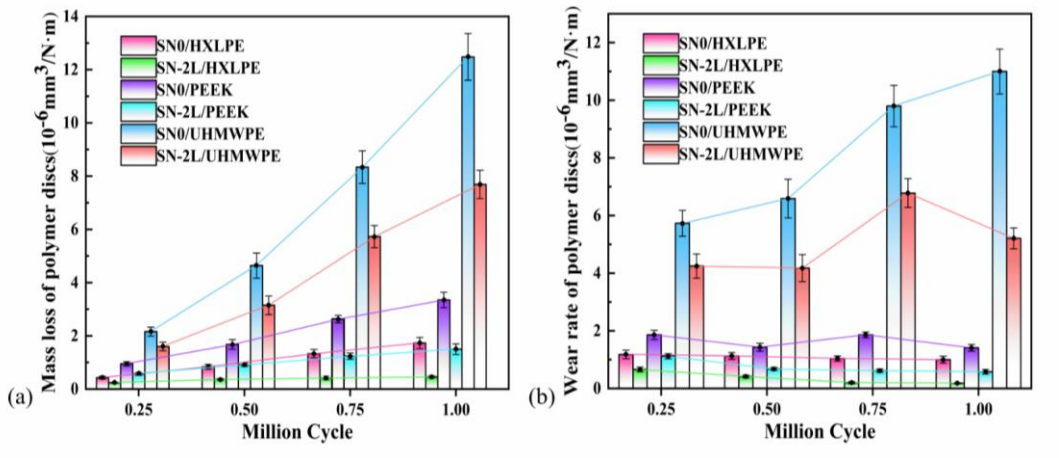

Figure 3: Mass loss (a) and wear rate(b) of polymer discs against pins at different wear stages.

Figure 4 shows the wear surface roughness of pin and disc samples at different wear stages. As can be seen from Figure 4 (a), when the cycle number is 1Mc, the surface roughness of SN-2L pin is significantly lower than that of SN0 pin. As can be seen from Figure 4 (b), the worn surface roughness of disc samples paired with SN-2L pin is also lower than that disc samples paired with SN0 pin. In particular, the worn surface roughness of disc samples paired with SN-2L pin tends to be stable (about Ra0.19μm) with the number of cycles, while the worn surface roughness of disc samples paired with SN0 pin increases significantly with the number of cycles.

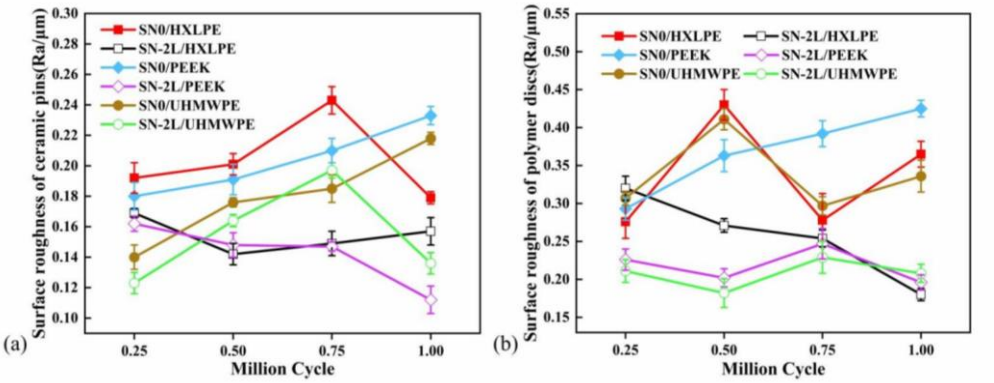

Figure 4: Surface roughness of ceramic pins (a) and polymer discs(b) at different wear stages.

Figure 5 shows the wear surface morphologies of SN0/polymer pairs. The wear surface morphologies of SN0/HXLPE pair can be seen from Figure 5-I and 5-II. It can be seen from the figures that, the wear surface morphologies of SN0 discs sliding against HXPLE discs change little with the increase of the number of cycles, and is relatively smooth on the whole. The slight furrow morphology can be obviously seen on the wear surface of HXPLE disc sliding against SN0 pin. Figure 5-III and 5-IV show the wear surface morphology of SN0/PEEK pair. It can be seen from the figures that, the wear surface of SN0 pin sliding against PEEK slightly becomes rough with the increase of the number of cycles, and some spalling pits appear on the wear surface. The furrows and scratches

on the wear surface of PEEK discs sliding against SN0 pins were serious especially with the increase of the number of cycles. Figure 5-V and 5-VI show the wear surface morphology of SN0/UHMWPE pair. It can be seen from the figures that, the wear surface of SN0 pin sliding against UHMWPE also becomes rough with the increase of the number of cycles. The wear surface of the UHMWPE disc with the increase of the number of cycles appears to crack and spalling in a large area.

Figure 6 shows the wear surface morphologies of SN-2L/polymer pairs. The wear surface morphologies of SN-2L/HXLPE pair can be seen in Figure 6-I and 6-II. As the number of cycles increases, the wear surface gradually becomes smooth. In particular, when the number of cycles is 1Mc, an obvious black surface film appears on the wear surface of the SN-2L pin sliding against HXPLE (see the yellow circle mark in Figure 6-I). The wear surface morphologies of SN-2L/PEEK pair can be seen in Figure 6-III and 6-IV. With the increase of cycles, the surfaces of the pin and disc change little with the increase of the number of cycles. At the same time, no surface film is found on the wear surface of SN-2L pin sliding against PEEK. The wear surface morphologies of SN-2L/UMWPE pair can be seen from Figure 6-V and 6-VI. As can be seen from the figures, the wear surfaces of the pin and disc becomes slightly rough, and no black surface film is found, too.

The surface film region on the wear surface of the SN-2L pin against HXPLE disc (the area inside the yellow circle in Figure 6-I) is observed in magnification, and the corresponding EDS analysis is performed, as shown in Figure 7. As can be seen from Figure 7(a), the surface of SN-2L pin specimen is indeed covered by a black surface film. Line scanning analysis is performed on the surface film region and non-surface film region (red line segment). As shown in Figure 7 (b), the contents of C and O elements in the surface film region are significantly higher than those in the non-surface film region. The results show that, the black film on the wear surface of SN-2L pin against HXPLE should contain a large amount of carbon-rich substances, oxides or hydroxides.

In order to further clarify the material composition of the surface film on the wear surface of SN-2L pin against HXLPE, XPS analysis is performed on the wear surface, and the results are shown in Fig. 8. As can be seen from Fig. 8 (a), the C1s peaks can be divided into three chemical states: C=C (282.8eV), C-N (284.2eV) and C=O (286.5eV), and the corresponding substances are polyethylene, N-GQDs [24] and carbonate. As can be seen from Fig. 8 (b), the Si2p peaks can be divided into three chemical peaks: Si simple substance (99.8eV), Si_3N_4 (101.2eV) and $SiO_2 \cdot nH_2O$ (105.2eV). As can be seen from Fig. 8(c), the O1s peaks can be divided into three spectral peaks with binding energy of 529.5eV (corresponding to metal oxides), 530.5eV (corresponding to metal carbonate) and 533.7eV (corresponding to SiO_2). XPS analysis results show that carbon-rich substances and tribo-chemical reaction products (such as $SiO_2 \cdot nH_2O$ and SiO_2) are formed on the wear surface of SN-2L pin against HXLPE.

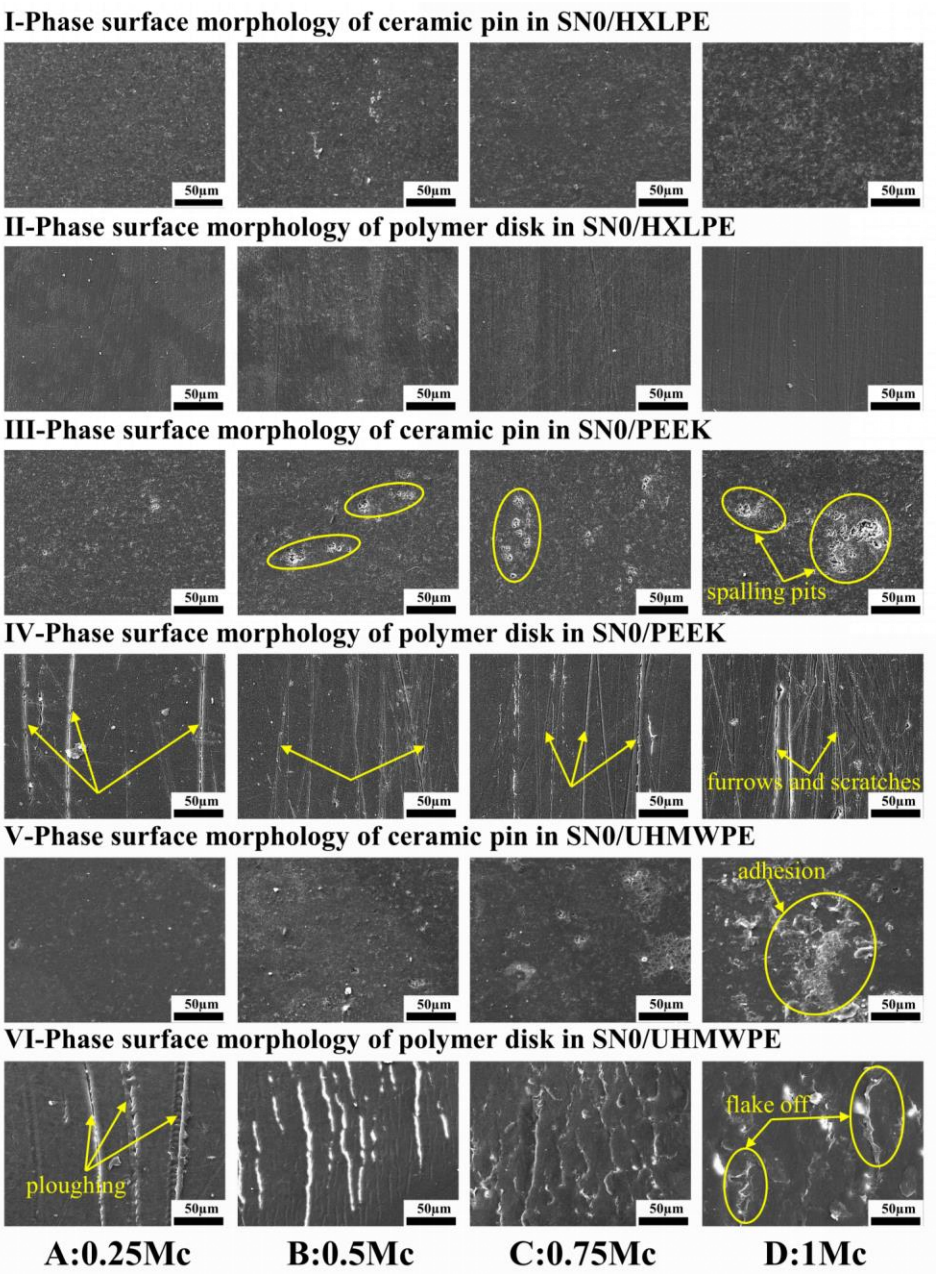

Figure 5: Wear morphologies of pins and discs in different wear cycles when SN0 slid against three kinds of polymers. A:0.25Mc, B:0.3Mc, C:0.75Mc and D:1Mc.

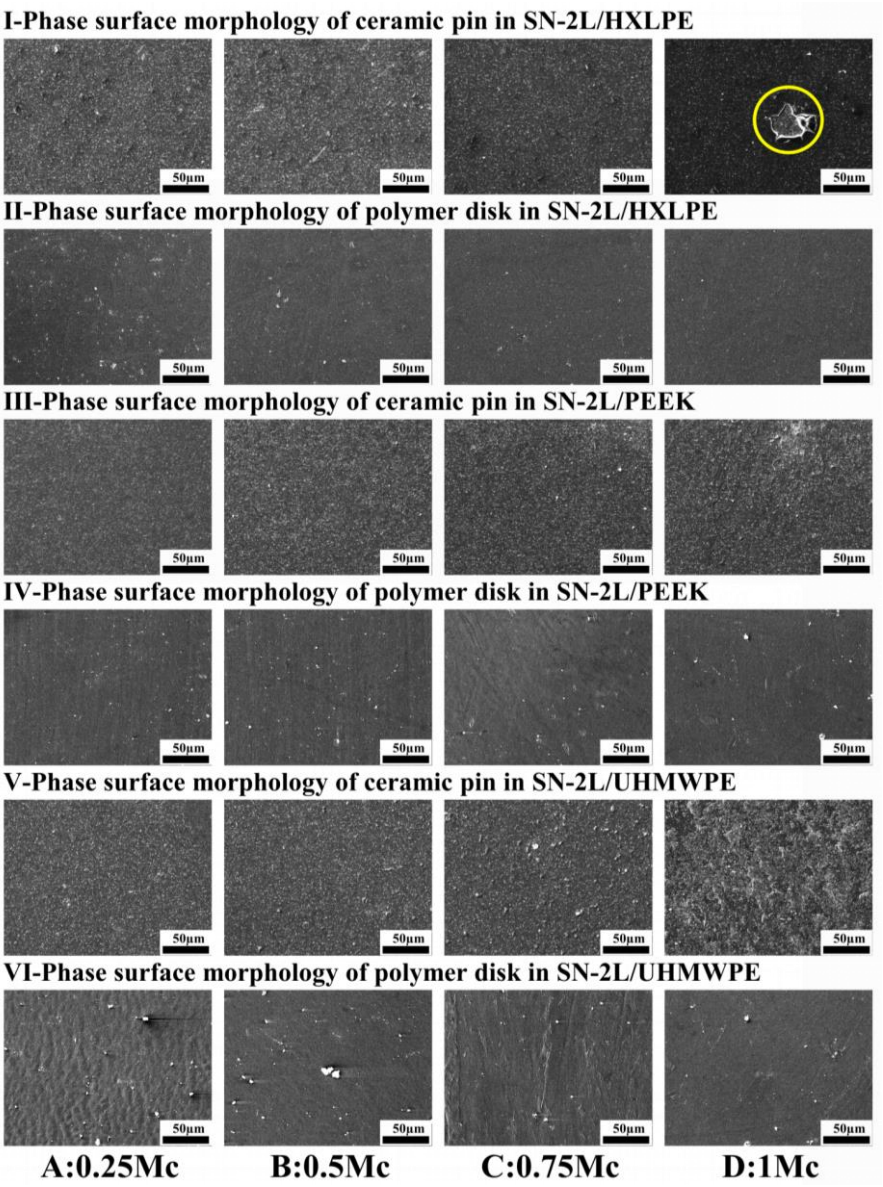

Figure 6: Wear morphologies of pins and discs in different wear cycles when SN-2L slid against three kinds of polymers. A:0.25Mc, B:0.3Mc, C:0.75Mc and D:1Mc.

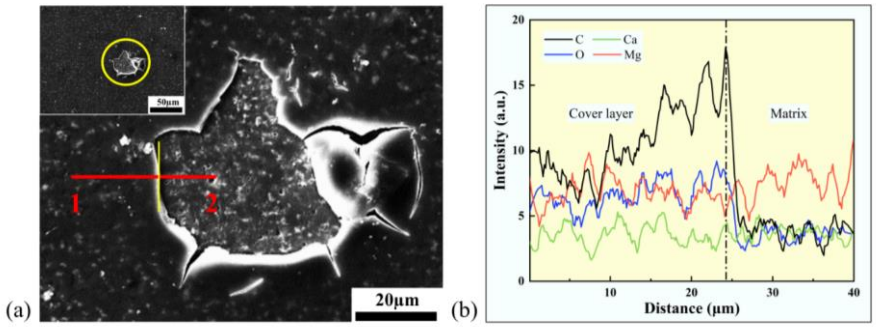

Figure 7: Local magnification of ceramic pin in SN-2L/HXLPE pair (a) and EDS analysis of specific area (b).

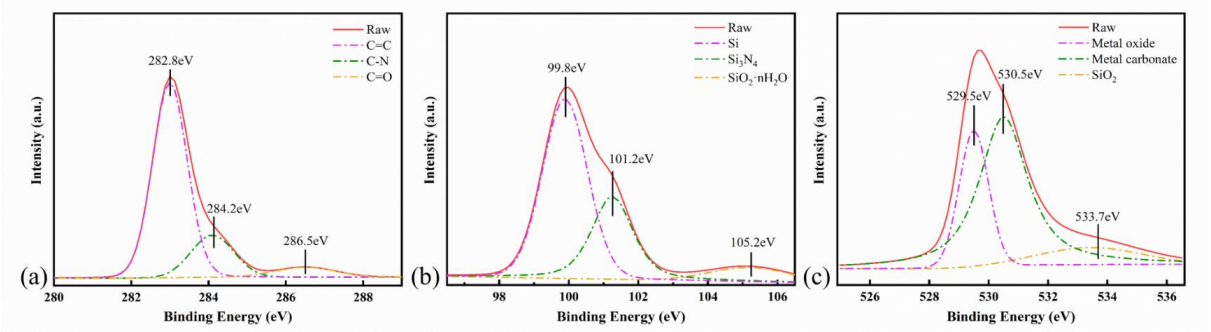

Figure 8: XPS analysis of the surface film on SN-2L in Fig.6-I (b): (a) C1s fitted peak spectra, (b) Si2p fitted peak spectra, (c) O1s fitted peak spectra.

Further, Raman spectrum analysis is performed on the wear surface of the polymer discs sliding against SN-2L pin (after 1Mc cycles), and the results are shown in Fig. 9. As can be seen from the figure, the characteristic peaks at 227cm^{-1}, 1350cm^{-1} and 1582cm^{-1} are detected on the wear surface of the polymer discs sliding against SN-2L pin. SiO_2 is the corresponding material at 227cm^{-1}, and the latter two correspond to the D and G peaks of the graphene material respectively. Among them, the intensity ratio (ID/IG) of the D-peak and G-peak on the HXPLE wear surface sliding against SN-2L is 0.55, and the ID/IG values on the PEEK and UHMWPE wear surface sliding against SN-2L are 0.74 and 0.84, respectively. The analysis results show that, the surfaces of SN-2L/polymer pairs form the tribo-chemical reaction products SiO_2 and defective graphene, and the wear surfaces of SN-2L/HXPLE pair represent the lowest ID/IG value and the least defects. In addition, Raman spectral analysis results also show the spectral peaks of $SiO_2 \cdot nH_2O$ (peak at 485cm^{-1}), and $Mg(OH)_2$ (peak at 276cm^{-1}) and $CaCO_3$ (peak at 708cm^{-1}) from calf serum.

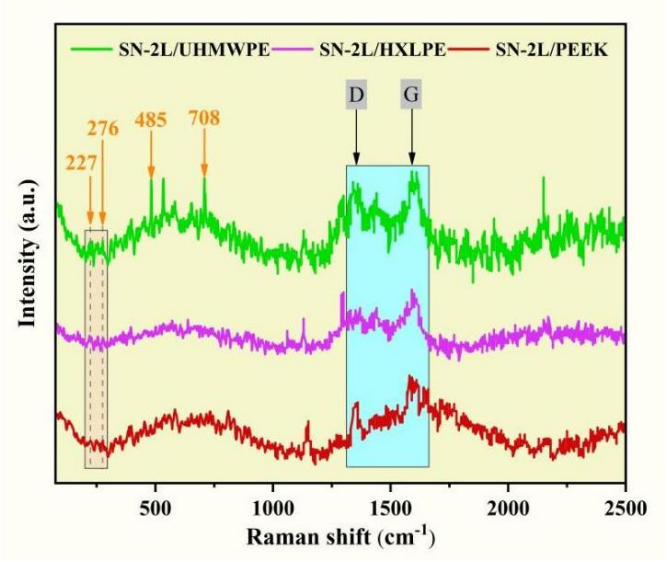

Figure 9: Raman spectroscopic analysis of wear surfaces of polymer discs sliding against SN-2L after 1Mc cycles.

Based on the above analysis results, it can be inferred that the black surface film formed on the wear surface of SN-2L pin against HXPLE is mainly composed of N-GQDs, SiO_2 and $SiO_2 \cdot nH_2O$. According to the analysis, when the SN-2L pin slides against HXLPE, in the initial friction stage, the surface micro-convex of the pin and disc contact under the action of normal load, as schematically

shown in Fig. 10 (a). With the progress of friction, the wear surface of the ceramic composite pin is slightly convex to plough the HXLPE disc, and part of the N-GQDs in the wear surface of composite pin breaks away from the surface and enters the wear interface. N-GQDs can play a certain role in protecting and reducing friction on the wear surface, as schematically shown in Fig. 10 (b). In simulated joint body fluids, silicon nitride and water molecules can undergo tribo-chemical reaction to produce silica gel [30].The tribo-chemical reaction can chemically polish the surface of the composite ceramic pin and make it more and more smooth. At the same time, silica gel and N-GQDs accumulate between the wear interface to play a further anti-friction and protective role, as schematically shown in Fig. 10 (c). As the pin and disc samples gradually become smooth, silica gel and N-GQDs are further enriched and dragged to form a surface film. When the cycle times reach 1Mc, a black surface film containing silica gel and N-GQDs is formed on the wear surface. In this case, most of the normal load is borne by the surface film and the hydrodynamic pressure film, which avoids direct contact with the micro-convex body of the wear surface of SN-2L pin and HXLPE disc, and reduces the wear rate of HXLPE to $0.18\times10^{-6}mm^3/N\cdot m$, as schematically shown in Fig. 10 (d).

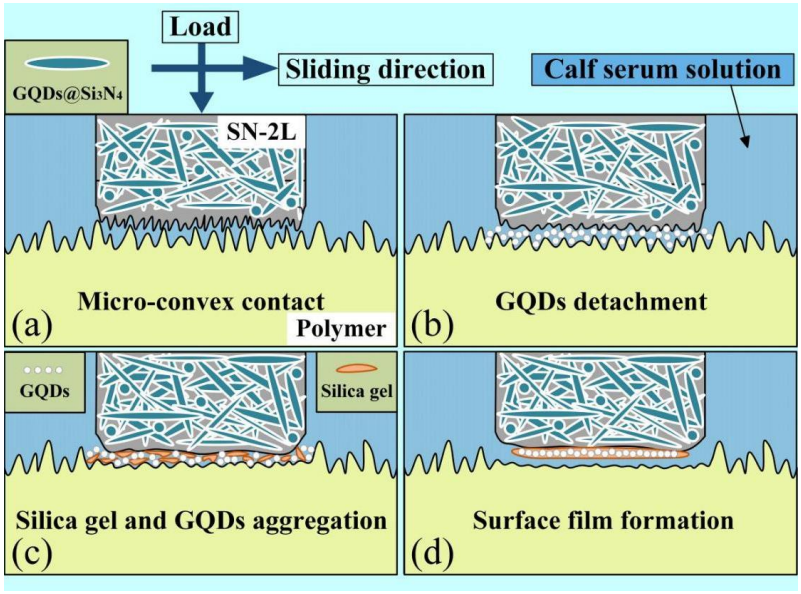

Figure 10: Schematic diagram of formation process of surface film on the wear surface of SN-2/HXLPE pair.

When SN-2L pin slides against polymer discs, its comprehensive mechanical properties are obviously better than SN0, so the wear surface of SN-2L pin has no serious damage, which is more conducive to better wear properties of SN-2L/polymer pairs. When the polymer disc is HXLPE, HXLPE is a more stable three-dimensional network structure obtained after radiation cross-linking of UHMWPE, which limits the movement of its molecular chain, reducing plastic deformation and reducing wear rate [31,32]. Therefore, during the wear process, the plastic deformation and damage on the wear surface of HXPLE against SN-2L pin are smaller, which can provide the condition to the formation of surface film composed of tribo-chemical reaction products and N-GQDs. So, the wear rate of HXLPE disc is as low as $0.18\times10^{-6}mm^3/N\cdot m$. Comparatively, UHMWPE is a two-dimensional linear structure, and its molecular chains are more prone to slip deformation under external forces. During the wear process, the wear surface of UHMWPE disc is prone to deformation, spalling and damage, and it is difficult to make the pair enter the state of fluid lubrication. Therefore, the wear

surface is relatively rough, and the wear rate is as high as $5.21\times10^{-6}mm^3/N\cdot m$. PEEK disc has higher hardness, but its plasticity is inferior to HXLPE. In the wear process, the wear surface of PEEK disc is easy to appear obvious furrow marks due to ploughing, which hinders the formation of effective surface film, and makes its wear rate slightly higher than that of HXLPE to $0.58\times10^{-6}mm^3/N\cdot m$.

When SN0 pin slides against polymer discs, due to the absence of N-GQDs, no such antifriction substance can play an effective antifriction and protection role. Even if the chemical product - silica gel is formed between the wear interface of the SN0/ polymer pair, a stable and effective surface film cannot be formed. Therefore, the overall wear of SN0 pin and polymer disc samples is worse, and the wear resistance of the sliding pair is poor.

In summary, the ceramic composites doped with 2wt% nano lignin have outstanding mechanical properties, but also exhibit excellent bio-tribological properties. It has great application potential in the field of artificial hip replacement materials.

4. Conclusions

In this paper, single-phase silicon nitride as a control group was used to systematically study the wear behavior of Si_3N_4-based composite containing N-GQDs against polymer in calf serum environment, and the following conclusions were obtained.

When SN-2L composite slid against polymer, the wear performances of the sliding pair were better than those of SN0/polymer pair because of the better mechanical properties and presence of N-GQDs of the ceramic composite. After 1Mc cycle, the wear surface of the pin and disc samples showed ultra-low damage degree. Compared with SN0/polymer pairs, the wear rates of HXLPE, UHMWPE and PEEK discs were reduced by 82%, 53% and 59%, respectively.

When SN-2L pin slid against HXLPE disc, a black surface film containing tribo-chemical product (silica gel) and N-GQDs formed on the wear surfaces of HXLPE disc. This surface film inhibited the direct surface contact between SN-2L pin and HXLPE disc, and the ultra-low wear rate of disc of $0.18\times10^{-6}mm^3/N\cdot m$ was obtained.

Declaration of competing interest

The authors declare that they have no known competing financial interests or personal relationships that could have appeared to influence the work reported in this paper.

Acknowledgements

This work was financially supported by the National Natural Science Foundation of China (Grant No. 52175178), National Natural Science Foundation of China (Grant No. 22378252), the Youth Innovation Team of Shaanxi Universities (2024) and Natural Science Foundation of Shaanxi Province (Grant No. 2018JM5056).

References

[1] Ashkenazi I, Christensen T, Oakley C, Bosco J, Lajam C, Slover J, et al. Trends in Revision Total Hip Arthroplasty Cost, Revenue, and Contribution Margin 2011 to 2021. J Arthroplast. 2023;38: 34-38.

[2] Bernasek TL, Gill M, Herekar R, Lyons ST. Total Joint Replacement, Contemporary Concepts. In: Harrison EE, Ho NH, editors. Managing Cardiovascular Risk In Elective Total Joint Arthroplasty. Cham: Springer International

Publishing; 2023. p. 7-22.
[3] Allen Q, Raeymaekers B. Surface Texturing of Prosthetic Hip Implant Bearing Surfaces: A Review. J Tribol-Trans ASME. 2021;143: 17.
[4] Kong X, Hu X, Chai W. In vitro & in vivo investigation of the silicon nitride ceramic hip implant's safety and effectiveness evaluation. Journal of Orthopaedic Surgery and Research. 2022;17: 87.
[5] Webster TJ, Patel AA, Rahaman M, Bal BS. Anti-infective and osteointegration properties of silicon nitride, poly (ether ether ketone), and titanium implants. Acta Biomater. 2012;8: 4447-4454.
[6] Gorth DJ, Puckett S, Ercan B, Webster TJ, Rahaman M, Bal BS. Decreased bacteria activity on Si_3N_4 surfaces compared with PEEK or titanium. International journal of nanomedicine. 2012: 4829-4840.
[7] Bal BS, Khandkar A, Lakshminarayanan R, Clarke I, Hoffman AA, Rahaman MN. Testing of silicon nitride ceramic bearings for total hip arthroplasty. Journal of Biomedical Materials Research Part B: Applied Biomaterials: An Official Journal of The Society for Biomaterials, The Japanese Society for Biomaterials, and The Australian Society for Biomaterials and the Korean Society for Biomaterials. 2008;87: 447-454.
[8] Cappi B, Neuss S, Salber J, Telle R, Knüchel R, Fischer H. Cytocompatibility of high strength non-oxide ceramics. Journal of Biomedical Materials Research Part A: An Official Journal of The Society for Biomaterials, The Japanese Society for Biomaterials, and The Australian Society for Biomaterials and the Korean Society for Biomaterials. 2010; 93:67-76.
[9] Mazzocchi M, Gardini D, Traverso PL, Faga MG, Bellosi A. On the possibility of silicon nitride as a ceramic for structural orthopaedic implants. Part II: chemical stability and wear resistance in body environment. Journal of Materials Science: Materials in Medicine. 2008;19: 2889-2901.
[10] Bal BS, Rahaman MN. Orthopedic applications of silicon nitride ceramics. Acta Biomater. 2012;8: 2889-2898.
[11] Neumann A, Jahnke K, Maier HR, Ragoss C. Biocompatibilty of silicon nitride ceramic in vitro. A comparative fluorescence-microscopic and scanning electron-microscopic study. Laryngo- rhino- otologie. 2004;83: 845-851.
[12] Taylor R, Bernero J, Patel A, Brodke D, Khandkar A. Silicon nitride: a new material for spinal implants. Orthopaedic Proceedings: Bone & Joint; 2010. p. 133.
[13] Llorente J, Ramírez C, Belmonte M. High graphene fillers content for improving the tribological performance of silicon nitride-based ceramics. Wear. 2019;430: 183-190.
[14] Belmonte M, Ramírez C, Gonzalez-Julian J, Schneider J, Miranzo P, Osendi MI. The beneficial effect of graphene nanofillers on the tribological performance of ceramics. Carbon. 2013;61: 431-435.
[15] Hvizdoš P, Dusza J, Balázsi C. Tribological properties of Si3N4–graphene nanocomposites. Journal of the European Ceramic Society. 2013;33: 2359-2364.
[16] Rutkowski P, Stobierski L, Zientara D, Jaworska L, Klimczyk P, Urbanik M. The influence of the graphene additive on mechanical properties and wear of hot-pressed Si_3N_4 matrix composites. Journal of the European Ceramic Society. 2015;35: 87-94.
[17] Li J, Yan Q, Zhang X, Zhang J, Cai Z. Efficient conversion of lignin waste to high value bio-graphene oxide nanomaterials. Polymers. 2019;11: 623.
[18] Ishii T, Mori M, Hisayasu S, Tamura R, Ikuta Y, Fujishiro F, et al. Direct conversion of lignin to high-quality graphene-based materials via catalytic carbonization. RSC advances. 2021;11: 18702-18707.
[19] Liu F, Chen Y, Gao JM. Preparation and Characterization of Biobased Graphene from Kraft Lignin. Bioresources. 2017;12: 6545-6557.
[20] Temerov F, Belyaev A, Ankudze B, Pakkanen TT. Preparation and photoluminescence properties of graphene quantum dots by decomposition of graphene-encapsulated metal nanoparticles derived from Kraft lignin and transition metal salts. Journal of Luminescence. 2019;206: 403-411.
[21] Liu W, Ning C, Sang R, Hou Q, Ni Y. Lignin-derived graphene quantum dots from phosphous acid-assisted hydrothermal pretreatment and their application in photocatalysis. Industrial Crops and Products. 2021;171: 113963.
[22] Yan C, Hu X, Guan P, Hou T, Chen P, Wan D, et al. Highly biocompatible graphene quantum dots: green synthesis, toxicity comparison and fluorescence imaging. Journal of materials science. 2020;55: 1198-1215.
[23] Jegannathan P, Yousefi AT, Abd Karim MS, Kadri NA. Enhancement of graphene quantum dots based applications via optimum physical chemistry: a review. Biocybernetics and Biomedical Engineering. 2018;38: 481-497.
[24] Chen W, Xu E, Zhao Z, Wu C, Zhai Y, Liu X, et al. Study on mechanical and tribological behaviors of GQDs @ Si_3N_4 composite ceramics. Tribology International. 2023;179.
[25] A WC, A ZZ, A RL, B HL, A NH. Study on self-derived products of nanometer lignin in silicon nitride ceramics during sintering process. 2021. Results in Materials. 12.

[26] Non-active surgical implants - Joint replacement implants - Particular requirements (ISO 21534:2007). 2009.
[27] Implants for surgery — Wear of total hip-joint prostheses — Part 1: Loading and displacement parameters for wear-testing machines and corresponding environmental conditions for test. ISO/TC 150/SC 4; 2014.
[28] Standard Test Method for Wear Testing of Polymeric Materials Used in Total Joint Prostheses. F04.15; 2011.
[29] Implants for surgery — Wear of total hip-joint prostheses — Part 2: Methods of measurement. ISO/TC 150/SC 4; 2016.
[30] Xu J, Kato K. Formation of tribochemical layer of ceramics sliding in water and its role for low friction. Wear: an International Journal on the Science and Technology of Friction, Lubrication and Wear. 2000: 245.
[31] Wang ZR, Li Q, Chen XC, Zhang Q, Wang K. High crystallinity makes excellent wear resistance in crosslinked UHMWPE. Polymer. 2023;280: 7.
[32] Huang YF, Zhang ZC, Xu JZ, Xu L, Zhong GJ, He BX, et al. Simultaneously improving wear resistance and mechanical performance of ultrahigh molecular weight polyethylene via cross-linking and structural manipulation. Polymer. 2016: 222-231.